

Article

Synergistic Removal of Nitrogen and Phosphorus in Constructed Wetlands Enhanced by Sponge Iron

Yiwei Shen ¹, Meijia Hu ¹, Yishen Xu ¹, Mengni Tao ¹, Lin Guan ², Yu Kong ², Shiwei Cao ¹ and Zhaoqian Jing ^{1,*}

¹ College of Civil Engineering, Nanjing Forestry University, Nanjing 210037, China; yiweishe@163.com (Y.S.); mengnitao@njfu.edu.cn (M.T.); cswxy@njfu.edu.cn (S.C.)

² Nanjing Municipal Design and Research Institute Co., Ltd., Nanjing 210008, China; glnjwater@163.com (L.G.); njszkongyu123@163.com (Y.K.)

* Correspondence: zqjing@njfu.edu.cn

Abstract: Insufficient denitrification and limited phosphorus uptake hinder nitrogen and phosphorus removal in constructed wetlands (CWs). Sponge iron is a promising material for the removal of phosphorus and nitrogen because of its strong reducing power, high electronegativity, and inexpensive cost. The influence of factors including initial solution pH, dosage, and the Fe/C ratio was investigated. A vertical flow CW with sponge iron (CW-I) was established, and a traditional gravel bed (CW-G) was used as a control group. The kinetic analysis demonstrated that for both nitrogen and phosphorus, pseudo-second-order kinetics were superior. The theoretical adsorption capacities of sponge iron for nitrate (NO_3^- -N) and phosphate (PO_4^{3-} -P) were 1294.5 mg/kg and 583.6 mg/kg, respectively. Under different hydraulic retention times (HRT), CW-I had better total nitrogen (TN) and total phosphorus (TP) removal efficiencies (6.08–15.18% and 5.00–20.67%, respectively) than CW-G. The enhancing effect of sponge iron on nitrogen and phosphorus removal was best when HRT was 48 h. The increase in HRT improved not only the nitrogen and phosphorus removal effects of CWs but also the reduction capacity of iron and the phosphorus removal effect. The main mechanisms of synergistic nitrogen and phosphorus removal were chemical reduction, ion exchange, electrostatic adsorption, and precipitation formation.

Keywords: sponge iron; synergistic removal; constructed wetland; nitrogen; phosphate



Citation: Shen, Y.; Hu, M.; Xu, Y.; Tao, M.; Guan, L.; Kong, Y.; Cao, S.; Jing, Z. Synergistic Removal of Nitrogen and Phosphorus in Constructed Wetlands Enhanced by Sponge Iron. *Water* **2024**, *16*, 1414. <https://doi.org/10.3390/w16101414>

Academic Editor: Alexandre T. Paulino

Received: 14 April 2024

Revised: 13 May 2024

Accepted: 14 May 2024

Published: 16 May 2024



Copyright: © 2024 by the authors. Licensee MDPI, Basel, Switzerland. This article is an open access article distributed under the terms and conditions of the Creative Commons Attribution (CC BY) license (<https://creativecommons.org/licenses/by/4.0/>).

1. Introduction

The excessive discharge of industrial, domestic, and agricultural wastes, as well as the increased utilization of chemical fertilizers in agriculture, can result in the accumulation of nitrogen (N) and phosphorus (P) in both groundwater and surface water [1]. While these nutrients are essential for aquatic organisms to thrive, an overabundance of them can cause eutrophication of the receiving water body, leading to water quality degradation [2,3]. High levels of nitrogen and phosphorus lead to excessive algae blooms, which result in excessive consumption of dissolved oxygen in water, reducing aquatic biodiversity and increasing the presence of harmful bacteria and toxins [4]. The presence of high levels of NH_4^+ in water can consume a large amount of disinfectant and form various nitrogen-containing disinfection byproducts, such as nitrosamines, nitramines, nitriles, nitroalkanes, and nitroaromatics [5,6]. Furthermore, the presence of residual NH_4^+ in the municipal water distribution networks will facilitate the proliferation of bacteria, thus further deteriorating water quality [7]. Prolonged exposure to water with high levels of NO_3^- can lead to a number of health problems, including gastrointestinal cancer, methemoglobinemia, and physiological abnormalities [8–10]. In addition, elevated concentrations of phosphorus in potable water can lead to a variety of symptoms, including fatigue, cramps in the hands and feet, dysuria, and renal impairment. Consequently, it is becoming increasingly evident that there is an urgent requirement to address the excessive levels of nitrogen and phosphorus in water.

The most commonly employed techniques for removing nitrate include reverse osmosis, ion exchange, chemical reduction, and biological denitrification [11–13]. While reverse osmosis and ion exchange are effective processes, they are expensive and also result in wastewater that requires additional treatment due to its high salt content [14]. The most popular treatment technique is biological denitrification, which offers the benefits of low energy consumption and environmental sustainability [15,16]. However, due to the insufficient carbon source in the secondary effluent of sewage treatment plants, the denitrification performance of the biological method cannot be further improved [17,18]. The chemical reduction method is simple, convenient, and fast, but it requires the continuous addition of a reducing agent. Zero-valent iron (ZVI) is often used as an electron donor to reduce nitrate in water, but its reduction product, ammonia nitrogen, needs to be further removed [19]. A variety of physical, chemical, and biological techniques have been proposed for the removal of phosphate from effluent. These include anion exchange, adsorption, reverse osmosis, chemical precipitation, membrane nanofiltration, electrodialysis, activated sludge systems, microalgae systems, and constructed wetlands [20–22]. In actual wastewater treatment plants, the most widely used method is chemical dephosphorization and the chemical agent utilized most frequently is iron. Xue et al. used sponge iron to remove phosphate in water and found that phosphate could be removed by chemically binding to Fe^{3+} or Fe^{2+} [23]. Thus, iron is an excellent substance for removing phosphorus and nitrogen at exactly the same time. Iron is an inorganic component that is ubiquitously present in the environment and plays a critical role in the C, O, N, and S cycles, either through chemical or microbial processes [24]. In addition, iron is an important redox component with a standard oxidation-reduction potential ($E_0 = -0.44 \text{ V}$). ZVI is a typical iron that has been extensively used in wastewater treatment [25]. It is non-toxic, inexpensive, and, most importantly, highly reactive. The characteristics of sponge iron as a novel type of inorganic porous metal composite material include low cost, high porosity, being difficult to cement, large specific surface area, and high active iron content. Compared with ZVI, sponge iron has stronger electrochemical enrichment, physical adsorption, and redox properties [26]. Therefore, in this study, sponge iron and CWs were combined to remove pollutants from wastewater treatment plant effluent to achieve the dual objectives of simultaneous phosphorus and nitrogen removal. The effects of dosage, the addition of activated carbon, pH, and other variables on the ability of the composites to remove nitrate and phosphate simultaneously were investigated. Combined with CWs operation and characterization of materials by SEM, XRD, and FTIR, the function of sponge iron in CWs was analyzed.

2. Materials and Methods

2.1. Systems Operation and Materials

The experiment established two laboratory-scale vertical upward-flow constructed wetland systems (CW-I, CW-G), and the device was 55 cm in height and had an interior diameter of 30 cm, composed of biological glass, as illustrated in Figure 1. The overall volume of the device was 40.25 L and the effective volume was about 21.5 L. Yellow calamus was planted in the device, with 4–5 robust plants per unit. The main body of CW-G was filled from top to bottom with 15 cm gravel, 10 cm sand, and 25 cm gravel successively, with gravel particle sizes of 8–12 mm and sand particle sizes of 0.5–2 mm. The installation of CW-I was identical to that of CW-G, with the addition of sponge iron above the sand layer. The composition of simulated effluent from the wastewater plant is as follows: $14.7 \pm 1.5 \text{ mg/L TN}$, $5.6 \pm 1.1 \text{ mg/L ammonia (NH}_4^+\text{-N)}$, $10.8 \pm 1.4 \text{ mg/L nitrate (NO}_3^-\text{-N)}$, and $0.5 \text{ mg/L TP (KH}_2\text{PO}_4)$. To change the pH of the simulated wastewater, 0.1 M NaOH and HCl were introduced.

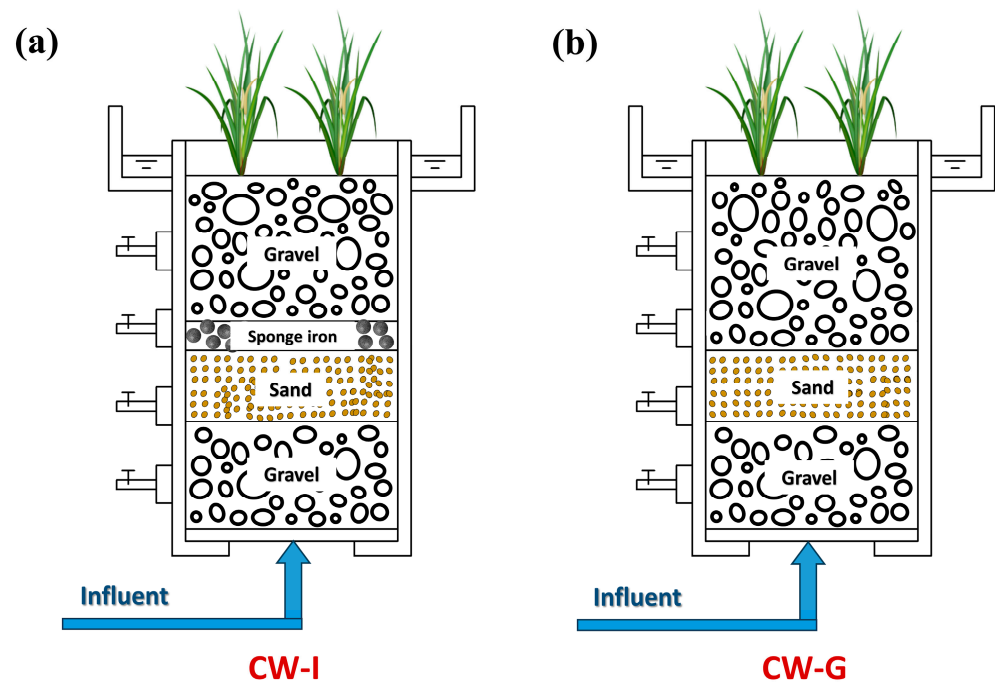


Figure 1. Installation of vertical flow constructed wetlands (CWs): (a) CW-I; (b) CW-G.

Sponge iron granules were bought from Miaoyuan Material Company (Zhengzhou, China), with particle sizes ranging from 1 to 3 mm. The iron content of the material is higher than or equal to 88%. The natural zeolite that was utilized as an adsorbent in this paper was produced in Jinyun (Zhejiang, China) and the particles were between 1 and 2 mm in size. The coconut-shell activated carbon granules were produced by Miaoyuan Material Company (Zhengzhou, China) and the particles were between 1 and 3 mm in size. Before use, the materials were repeatedly cleaned with deionized water (DI) after being rinsed multiple times with tap water, and then dried for 10 h in a 90 °C oven.

2.2. Experimental Methods of Influencing Factors

The influences of different initial pH (3–10), dosage (0.5–3 g), and different Fe/C ratios on the simultaneous elimination of phosphorus and nitrogen were investigated. Taking the experimental influence of dosage addition as an example: In a series of 250 mL conical flasks, 0.5, 1.0, 1.5, 2.0, 2.5, and 3.0 g of sponge iron were, respectively, added to 100 mL of simulated wastewater, along with an appropriate amount of zeolite to mitigate the impact of ammonia nitrogen accumulation. The pH was adjusted to 7, and the flasks were set up in an oscillator with a reciprocating constant temperature and shaken at a speed of 160 rpm/min for 24 h. The supernatant obtained after adsorption was filtered past a 0.45 µm water-filtering membrane. Then, the removal rate was calculated and analyzed.

2.3. Adsorption Experiments Methods

2.3.1. Adsorption Kinetics

In a thermostatic water-bath shaker, the adsorption kinetics studies were carried out using appropriate amounts of sponge iron and 100 mL of simulated wastewater (160 rpm). The adsorption capacity at different times (5 min–24 h) was investigated at 25 °C. The reaction water sample was filtered using a 0.45 µm filter membrane in order to measure the concentration of TN and $\text{PO}_4^{3-}\text{-P}$ in the supernatant. Both the pseudo-second-order and pseudo-first-order kinetic models were able to fit the adsorption experimental results of $\text{PO}_4^{3-}\text{-P}$ and TN, respectively. The adsorption mechanism was also analyzed using the intraparticle diffusion model.

2.3.2. Equilibrium Isotherms

In order to carry out the equilibrium isothermal adsorption experiments, 100 mL of solution and the required quantities of sponge iron were placed in a 250 mL Erlenmeyer flask and shaken in a thermostatic water-bath shaker (160 rpm) at 25 °C. Aqueous solutions of NO_3^- -N were controlled at concentrations of 5, 10, 20, 50, 72, 100, 120, 160, and 200 mg/L. Aqueous solutions of PO_4^{3-} -P were controlled at concentrations of 0.25, 0.5, 1.0, 2.5, 3.6, 5.0, 6.0, 8.0, and 10 mg/L. All of the suspensions were brought to an initial pH of 7 by adding a small amount of 0.1 M HCl solution. Following the reaction, the experimental water samples were filtered by membrane filters with a pore size of 0.45 μm in order to measure the residual concentrations of NO_3^- -N and PO_4^{3-} -P from the supernatant. Three distinct isothermal equations, Freundlich, Langmuir, and Temkin, were used for the fitting and analysis of the test data.

2.4. Analysis and Characterization Methods

The surface morphology of sponge iron was analyzed at different pH levels both before and after the reaction by field-emission scanning electron microscopy (SEM; Quanta 200, FEI, Hillsboro, OR, USA). Firstly, dry the samples, then use conductive adhesive to stick them onto the sample board for gold spraying treatment, and observe the surface characteristics of samples under a certain magnification. X-ray diffractometry (XRD; Ultima IV, Rigaku, Tokyo, Japan) analysis was used to infer the crystal structure, including the lattice constant, interatomic distance, and atomic arrangement in the crystal, by measuring the position and intensity of characteristic diffraction peaks. The surface functional groups of SI before and after the reaction were analyzed using an infrared spectrometer (FTIR; VERTEX 80 V, Bruker, Ettlingen, Germany) to analyze the mechanism and the frequency range in which the spectra were captured (500–4000 cm^{-1}).

3. Results and Discussion

3.1. Influence of Operating Factors

3.1.1. Dosage of Sponge Iron

The influence of sponge iron dosage on the removal efficiency of nitrate and phosphate at room temperature is shown in Figure 2a,b. As the dosage of sponge iron was increased, the corresponding removal rate of nitrate and phosphate showed an upward trend, while the removal capacity per unit mass steadily dropped. More active sites were made available by increasing the quantity of sponge iron per unit volume of solution, which effectively increased the overall surface area of sponge iron and also successfully improved the removal effectiveness of nitrate and phosphate [27]. When the dosage was 1.5 g, the removal percentages for nitrate and phosphate were 39.9% and 47.8%, respectively. Under these conditions, the residual phosphate concentration dropped below 0.3 mg/L. Then, as the amount of sponge iron continued to increase, the improvement in the removal rate was no longer obvious. When some pollutants were removed, the concentration of pollutants in the solution decreased, and the concentration difference between inside and outside the material surface decreased. At this time, continuing to increase the amount of sponge iron had little effect and would only cause material waste [28]. Therefore, the material dosage should be established based on the actual pollutant concentration in practical applications in order to achieve economic and practical purposes.

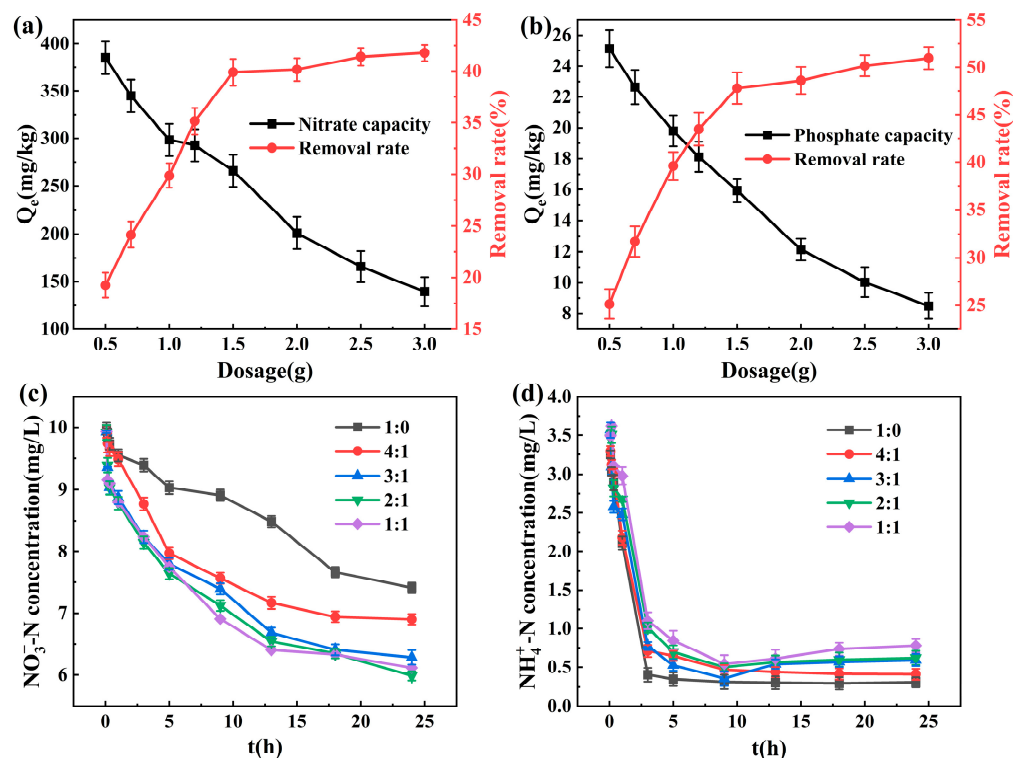


Figure 2. The effect of dosage on pollutant removal: (a) NO_3^- -N; (b) PO_4^{3-} -P. The effect of Fe/C ratios on pollutant removal: (c) NO_3^- -N; (d) NH_4^+ -N.

3.1.2. Fe/C Ratios

Figure 2c,d shows the concentration change of ammonia and nitrate with time under the condition of different Fe/C ratios of composite materials. Compared with the 1:0 group, the speed of nitrate removal was significantly accelerated by the addition of activated carbon. Because the redox reaction between nitrate and zero-valent iron is a heterogeneous reaction, and the reaction rate is slow, the larger the proportion of activated carbon added, the faster the elimination rate of nitrate and the more effective the result. The sponge iron was mixed with active carbon to form a galvanic cell system through potential difference, which caused micro-electrolysis, increasing the reaction active sites and electron transfer so as to improve the rate of chemical reaction [29]. Iron carbon micro-electrolysis can promote the electrochemical corrosion of sponge iron, which is a process that moves from thermodynamic instability to thermodynamic stability. Therefore, the oxidation–reduction reaction between iron and nitrate occurred, producing various iron complexes at the same time which can wrap nitrate, ammonia, or nitrite to achieve a certain removal effect [30]. When the Fe/C ratios exceeded 3:1, the rate advantage of nitrate removal was no longer obvious, yet the amount of nitrate in the solution kept decreasing, perhaps because the activated carbon itself had a certain adsorption effect on nitrate. As the amount of activated carbon grew, so did the number of adsorption active points and the removal rate. In a neutral electrolyte, sponge iron, with low potential, lost electrons and acted as an anode, while activated carbon, with high potential, acted as a cathode. The hydrogen atoms with strong reducing properties were created from the H^+ and H_2O adsorbed on the activated carbon surface after receiving electrons. The electric field effect caused NO_3^- -N in the solution to move to sponge iron, then reduced it to NH_4^+ -N. As seen in Figure 2d, the concentration of ammonia nitrogen decreased very rapidly during the experiment, which was attributed to the excellent ability of zeolite to adsorb cations. After 5 h, the remaining NH_4^+ -N concentration was less than 1 mg/L. When the proportion of activated carbon was too high and the reaction time exceeded 9 h, the ammonia concentration rose slightly. The ammonia generated by nitrate reduction cannot be absorbed in time since the

zeolite's adsorption capacity was getting close to saturation and the adsorption rate had dropped. Therefore, considering the removal effect and economy of nitrate and ammonia comprehensively, the subsequent experiments would be conducted according to the Fe/C ratio of 3:1.

3.1.3. Initial Solution pH

The effect of initial solution pH on simultaneous removal is illustrated in Figure 3. Simultaneous removal efficiency declined progressively as the initial pH increased. Ammonia nitrogen in solution was mainly removed by zeolite adsorption. Under alkaline conditions, a large amount of ammonia in the solution was converted into $\text{NH}_3 \cdot \text{H}_2\text{O}$, but the affinity of zeolite to $\text{NH}_3 \cdot \text{H}_2\text{O}$ in the solution was low, so ammonia elimination was significantly reduced. Under neutral and weak acids, ammonia nitrogen existed in the form of NH_4^+ , which was conducive to the ion exchange of zeolite. Sponge iron was more effective in removing nitrate under acidic conditions. With a rise in pH value, the removal rate dropped, and the whole reaction was an acid-flooding reaction [31]. Nitrate reduction would be prevented by the sponge iron's surface developing iron oxides in conditions of high pH value. Under alkaline conditions, the competition between OH^- and nitrate intensifies, resulting in electrostatic repulsion, which decreases the adsorption capacity. When pH changed from 6 to 8, there was hardly any change in the rate of nitrate elimination, which was congruent with the findings obtained by Guo et al. [32]. From Figure 3c,d, it can be seen that there was minimal difference in the removal rate of TN and NO_3^- -N at pH 5 and 6. In the process of reducing nitrate, iron would consume a considerable amount of hydrogen ions. Lower pH values and higher H^+ concentrations were beneficial for hydrogen evolution corrosion on sponge iron surfaces. The hydrogen atom with strong reducibility produced by hydrogen evolution corrosion can inhibit the generation of a passivation film on the surface of iron, thus speeding up the elimination of nitrate. Moreover, acidic conditions can also promote the conversion of iron into ferrous ions and facilitate the existence of ferrous ions. The presence of Fe^{2+} can promote the reduction effect of unacidified Fe^0 on NO_3^- [33].

The phosphate removal dropped dramatically as the pH rose, as illustrated in Figure 3a,b. The removal of phosphate in the sponge iron system mainly depended on its reaction with ferrous ions and iron ions generated by zero-valent iron oxidation to generate precipitation. The pH value affected the dissociation status and solubility of solutes, thus affecting the adsorption capacity. Low-pH conditions were conducive to the acceleration of Fe-C micro-electrolysis reactions and iron corrosion. Iron was corroded as an anode to generate Fe^{2+} , and H^+ generated H_2 or H_2O at the cathode. With the increase in solution pH, H_2O was reduced to OH^- as a cathode reactant. OH^- competed with phosphate ions to precipitate with iron ions or ferrous ions, thus affecting the phosphate removal rate. Furthermore, the oxide produced on the sponge iron surface and the hydroxyl iron oxide (FeOOH) generated by the reaction of Fe^{3+} with water have a certain adsorption capacity for phosphorus [34]. The mechanism of phosphorus removal from water by ferric oxide is mainly possible because ferric oxide has a positively charged surface, and electrostatic attraction is generated between the positively charged ferric oxide and the negatively charged phosphate ion surface in solution. The charge properties of the adsorbent surface were altered by the pH level. As the pH of the solution rose, the negative charge on the iron oxide surface steadily grew while the positive charge gradually decreased, which led to a gradual increase in electrostatic repulsive force between the negatively charged iron oxide surface and the negatively charged phosphate ion, reducing the unit adsorption amount of Fe_3O_4 to phosphorus [35].

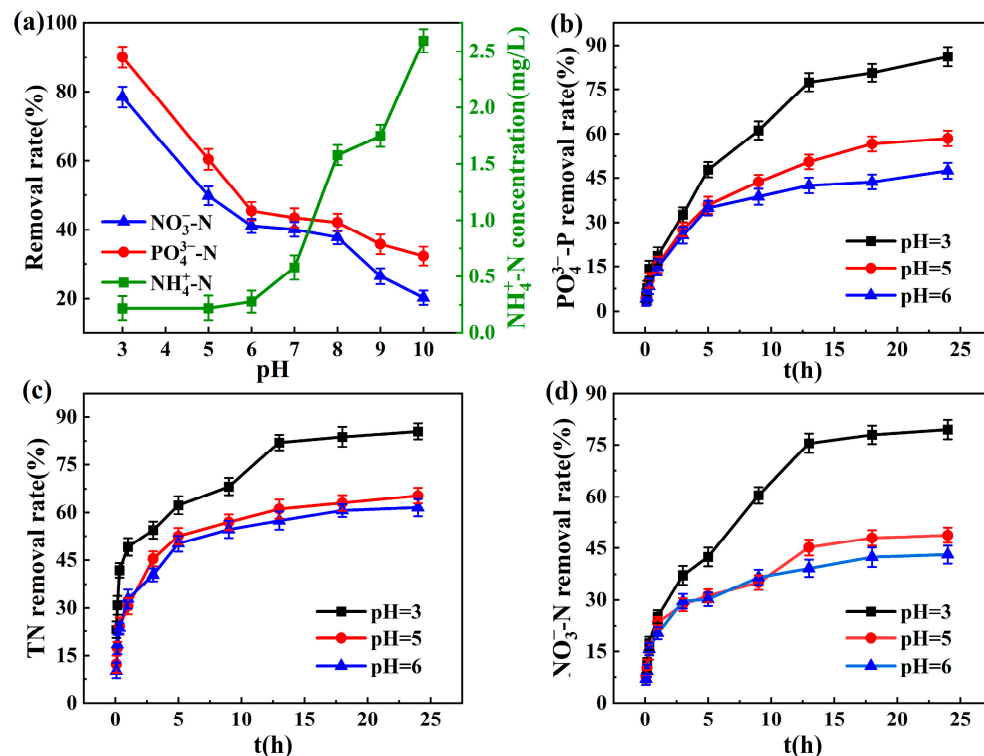


Figure 3. (a) Effect of initial pH on NO_3^- -N, NH_4^+ -N, and PO_4^{3-} -P co-removal efficiency; The kinetic effect of different initial pH levels on the removal of (b) PO_4^{3-} -P, (c) TN, and (d) NO_3^- -N.

3.2. Batch Adsorption Experiments

3.2.1. Adsorption Kinetics

To match the statistics of total nitrogen and phosphate elimination by the sponge iron, the pseudo-first-order adsorption kinetic, pseudo-second-order adsorption kinetic, and intra-particle diffusion models were analyzed. The results are shown in Figure 4, and Table 1 shows the parameters of the fitting models. The fitting results revealed that the pseudo-second-order kinetic model was better than the pseudo-first-order kinetic model for the simultaneous removal of total nitrogen and phosphate, demonstrating that complex chemical adsorption of phosphate and total nitrogen may occur in the sponge iron [36]. In addition, the correlation coefficients (R^2) of the pseudo-second-order model for total nitrogen and phosphate were 0.998 and 0.996, respectively. The actual values of total nitrogen and phosphate equilibrium adsorption, which were 185.185 mg/kg and 14.451 mg/kg, respectively, were close to the theoretical values. The fitting curves of intra-particle diffusion in the adsorption process are shown in Figure 4c,d to comprise three distinct stages: quick diffusion at the outside surface (membrane diffusion), diffusion at the inside surface, and dynamic adsorption equilibrium [37]. The intercept of the fitted lines was minimal in the initial phase, indicating that the border layer was thin in thickness and the likelihood of the surface mass transfer was higher. At this time, there was a large number of unoccupied adsorption sites, so a considerable proportion of nitrogen and phosphorus was rapidly removed. The key rate-regulating step of the pollutant adsorption process was the internal diffusion process, as evidenced by the fact that the K_{d2} value of the second phase was much lower than that of the first phase. The adsorption entered the final phase when susceptibility to diffusion inside the inner porosity continued to rise to a certain amount. In the third stage, between contaminants and adsorbents, an apparent dynamic equilibrium mechanism of adsorption–desorption predominated. In addition, the intra-particle diffusion fitting lines were unable to cross the zero point, indicating that the rate control process of the adsorption of nitrogen and phosphorus was not the only

intraparticle diffusion process but was also influenced by boundary layer diffusion and external surface adsorption [38].

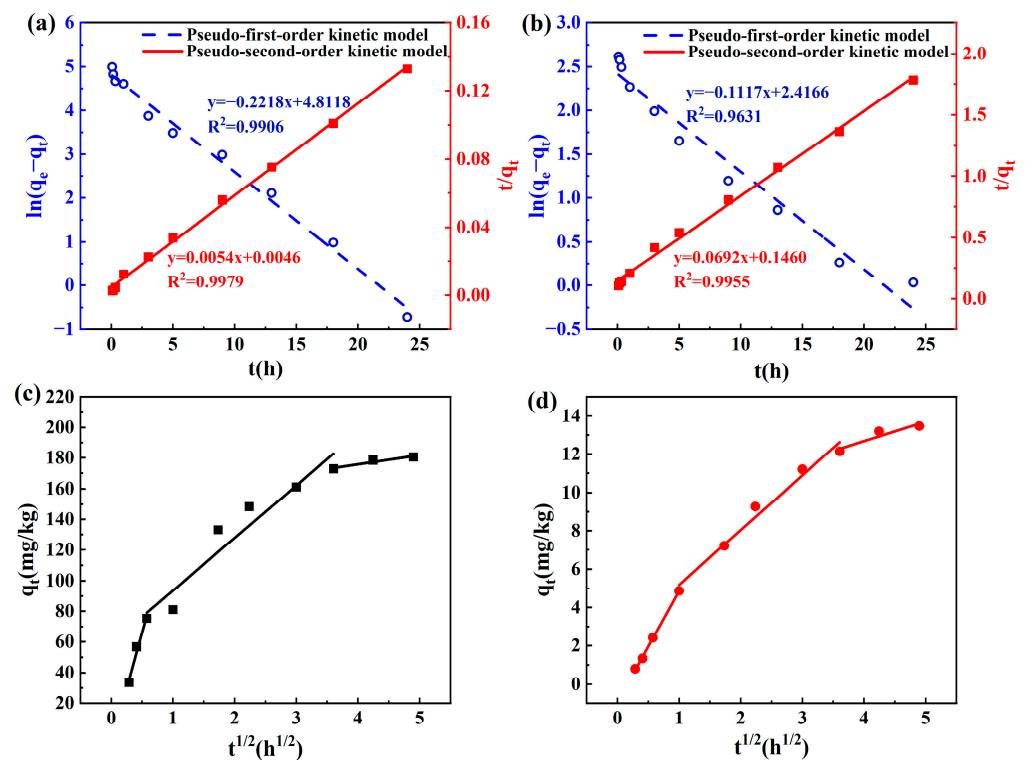


Figure 4. The kinetic fitting curves of (a) TN and (b) $\text{PO}_4^{3-}\text{-P}$; The intra-particle diffusion fitting curves of (c) TN and (d) $\text{PO}_4^{3-}\text{-P}$.

Table 1. The adsorption kinetics and intraparticle diffusion model parameters of sponge iron for co-adsorption of TN and $\text{PO}_4^{3-}\text{-P}$.

| | C_0 (mg/L) | q_{exp} (mg/kg) | Pseudo-First-Order | | | Pseudo-Second-Order | | |
|-----------------------------|-----------------|--|------------------------------|--|-------|--|-----------------------------|-------|
| | | | K_1 (h^{-1}) | q_{cal} (mg/kg) | R^2 | K_2 ($\text{kg}\cdot\text{mg}^{-1}\cdot\text{h}^{-1}$) | q_{cal} (mg/kg) | R^2 |
| TN | 15 | 860.676 | 0.172 | 603.050 | 0.980 | 0.001 | 909.091 | 0.999 |
| $\text{PO}_4^{3-}\text{-P}$ | 0.5 | 24.467 | 0.121 | 22.03 | 0.979 | 0.010 | 27.933 | 0.998 |
| Intra-Particle Diffusion | | | | | | | | |
| | C_0 (mg/L) | K_{d1} ($\text{mg}\cdot\text{kg}^{-1}\cdot\text{h}^{-0.5}$) | R^2 | K_{d2} ($\text{mg}\cdot\text{kg}^{-1}\cdot\text{h}^{-0.5}$) | R^2 | K_{d3} ($\text{mg}\cdot\text{kg}^{-1}\cdot\text{h}^{-0.5}$) | R^2 | |
| TN | 15 | 382.817 | 0.999 | 230.630 | 0.946 | 49.243 | 0.984 | |
| $\text{PO}_4^{3-}\text{-P}$ | 0.5 | 5.638 | 0.990 | 6.511 | 0.985 | 1.663 | 0.975 | |

3.2.2. Equilibrium Isotherms

In this paper, three distinct kinds of isothermal adsorption models were employed to match the data of nitrogen and phosphorus co-adsorption by sponge iron. The outcomes are displayed in Figure 5 and Table 2. Because of the significant difference in nitrate and phosphate concentrations between the sponge iron and its surrounding solution, it was possible to overcome the external mass transfer resistance, which led to an increase in adsorption capacity and caused a progressive stabilization as the starting concentration rose. A higher initial concentration can improve the contact rate between ions and adsorption sites on the adsorbent surface so that more nitrogen and phosphorus were adsorbed. According to the coefficients of correlation (R^2) and the fitting curve, it can be inferred that the adsorption mechanism of phosphate was more compatible with the Langmuir

adsorption isotherm than the Freundlich model, which extrapolated that the surface of the sponge iron included a relatively uniform distribution of energetic adsorption sites. The Q_m in the Langmuir isotherm model represented the maximal theoretical adsorption capacity, and the maximal theoretical adsorption capabilities of the sample for phosphate and nitrate were 0.584 mg/g and 1.294 mg/g, respectively. The Freundlich model for nitrate adsorption had a higher degree of fitting accuracy than the Langmuir model, indicating that the adsorbing process was relatively complicated. There might be surface corrosion flaws on the sample and the formation of a heterogeneous iron oxide surface during the adsorption process. Monolayer adsorption and multilayer adsorption existed simultaneously. The n in the Freundlich equation can reflect the degree of adsorption difficulty of materials. When $0.3 < 1/n < 1$, it means that the material is easily able to absorb nitrate and phosphate [39]. To characterize the adsorption of pollutants with significant ion exchange, the Temkin model was fitted. As a consequence, the correlation coefficient (R^2) of phosphate exceeded 0.9, manifesting that the removal process of PO_4^{3-} -P might involve strong ion exchange or electrostatic force [40,41]. The fitting degree of the Temkin model for phosphate adsorption was significantly higher than nitrate, indicating that phosphate adsorption was mainly achieved through chemical adsorption, while for nitrate, it was mainly through physical adsorption.

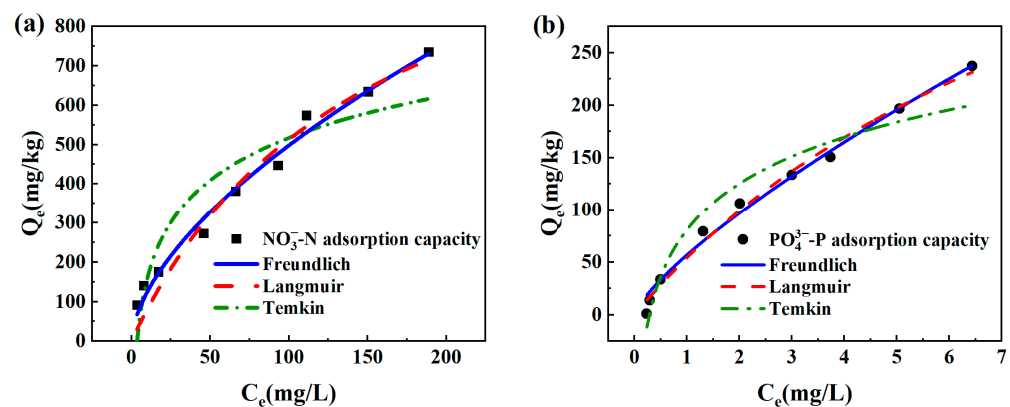


Figure 5. Adsorption isotherms of sponge iron fit by Langmuir, Freundlich, and Temkin for co-adsorption of (a) NO_3^- -N and (b) PO_4^{3-} -P.

Table 2. Isotherm calculation parameters of NO_3^- -N and PO_4^{3-} -P adsorbed on the sponge iron.

| | Langmuir | | | Freundlich | | | Temkin | | |
|----------------|-----------------|------------------|-------|---|-------|-------|---------|------------------|-------|
| | K_L (L/mg) | Q_m (mg/kg) | R^2 | K_F ($mg^{1-1/n} \cdot L^{1/n} \cdot kg^{-1}$) | $1/n$ | R^2 | K_T | A_T (mg/kg) | R^2 |
| NO_3^- -N | 0.007 | 1294.496 | 0.964 | 30.698 | 0.605 | 0.986 | 156.090 | 0.274 | 0.869 |
| PO_4^{3-} -P | 0.102 | 583.562 | 0.990 | 56.664 | 0.770 | 0.989 | 64.150 | 3.516 | 0.942 |

3.2.3. Reaction Mechanism

X-ray diffraction was utilized to ascertain the crystal structure of sponge iron particles (Figure 6a). Jade6.0 software and standard PDF card were used to find that the characteristic peaks at 2θ of 44.67° and 65.02° correspond to the (110) and (200) crystal planes of Fe^0 (PDF#06-0696), respectively, confirming the existence of Fe^0 . The characteristic peaks observed at 2θ of 30.24° , 35.63° , 43.28° , 57.27° , and 62.92° coincide with the (220), (311), (400), (511), and (440) crystallographic planes of Fe_2O_3 (PDF#39-1346), respectively. The composite's diffraction peaks were recorded at 2θ values of 31.25° , 36.82° , 44.76° , 55.62° , 65.18° , and 59.30° , and these values match to the (220), (311), (400), (422), (440), and (511) crystal planes of Fe_3O_4 (PDF#26-1136) [42]. Peaks of diffraction were seen at 2θ values of 18.90° , 31.10° , 13.02° , 36.65° , 44.56° , 59.02° , and 64.86° , which were consistent with

those of Spinel (PDF#89-5701), and the 2θ values of 17.35° , 22.87° , 23.86° , 25.43° , 32.30° , 35.70° , 36.50° , and 39.67° confirmed the presence of forsterite (PDF#83-0978), indicating that sponge iron contains a small amount of minerals. The XRD spectra revealed that the materials were mostly composed of some minerals, carbon, iron, and their oxides.

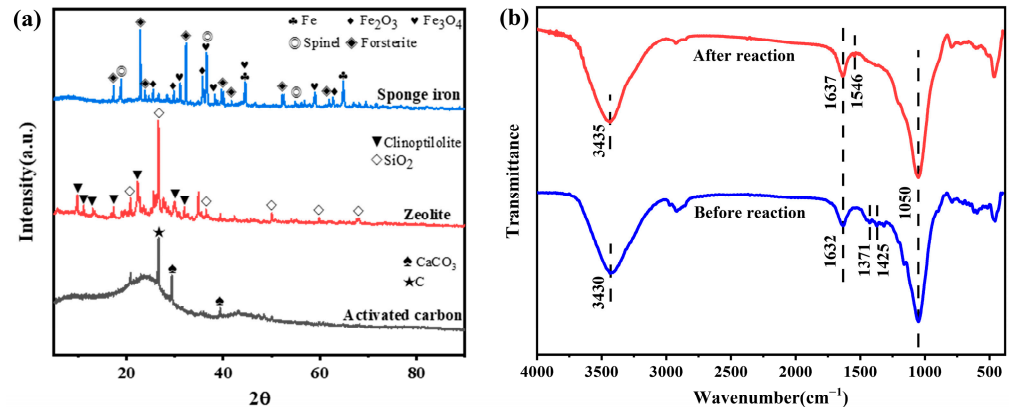


Figure 6. (a) XRD spectra of sponge iron and activated carbon; (b) FTIR spectra of the samples before and after co-removal.

The FTIR spectra of the materials before and after the co-removal of phosphate and nitrogen were acquired in the range of $400\text{--}4000\text{ cm}^{-1}$ (Figure 6b). The stretching vibration of O-H bonds and the blending vibration of adsorbed water were linked to the broad band in the vicinities of 3430 cm^{-1} and 1632 cm^{-1} , respectively. After the reaction, the characteristic spike at 3430 cm^{-1} was weakened and shifted to 3435 cm^{-1} , which might be caused by the complexation between an ammonium ion and a free O-H group, demonstrating that the hydroxyl group took part in the adsorption reaction of ammonia [43]. The chemisorption of NH_4^+ on the composite was demonstrated by the emergence of a new vibration band at 1546 cm^{-1} in the spectra following the reaction, which was the result of the stretching vibration of N-H bonds [44]. After the reaction, it was observed that the strength of the stretching vibration band of CO_3^{2-} was reduced near 1371 cm^{-1} and 1425 cm^{-1} . The decrease in the strength of CO_3^{2-} bands may signify that certain carbonate groups in the materials have been replaced by phosphate [45].

The surface appearance and pore structure of sponge iron particles before and after the reaction were examined by SEM (Figure 7). Before the experiment, there were micron-scale holes and fissures on the sponge iron surface (Figure 7A), and the inner surface of the pores was relatively flat, dense, and smooth (Figure 7a). After the experiment, it was clear that there had been a change in sponge iron surface morphology. Because the pores in the sponge iron at the micron scale were densely covered by crystalline precipitates, the sponge iron surface had numerous irregular holes (Figure 7(B,b)). These precipitates clogged the pores of the sponge iron, thereby reducing the number of catalytic sites. This might be what caused the reaction rate to decrease over time. After the reaction under acidic circumstances, the sponge iron surface had a significant amount of corrosion and its by-products (Figure 7c). Corrosion caused the sponge iron surface to become bumpy, indicating that more active sites were exposed to the surface. After the reaction under alkaline conditions, a considerable number of cluster crystals were observed on the sponge iron surface (Figure 7d). This indicated that a high pH value would promote the formation of crystallization on the sponge iron surface, which would block the pores and reduce the active sites, thus preventing the reaction of sponge iron with nitrogen and phosphorus.

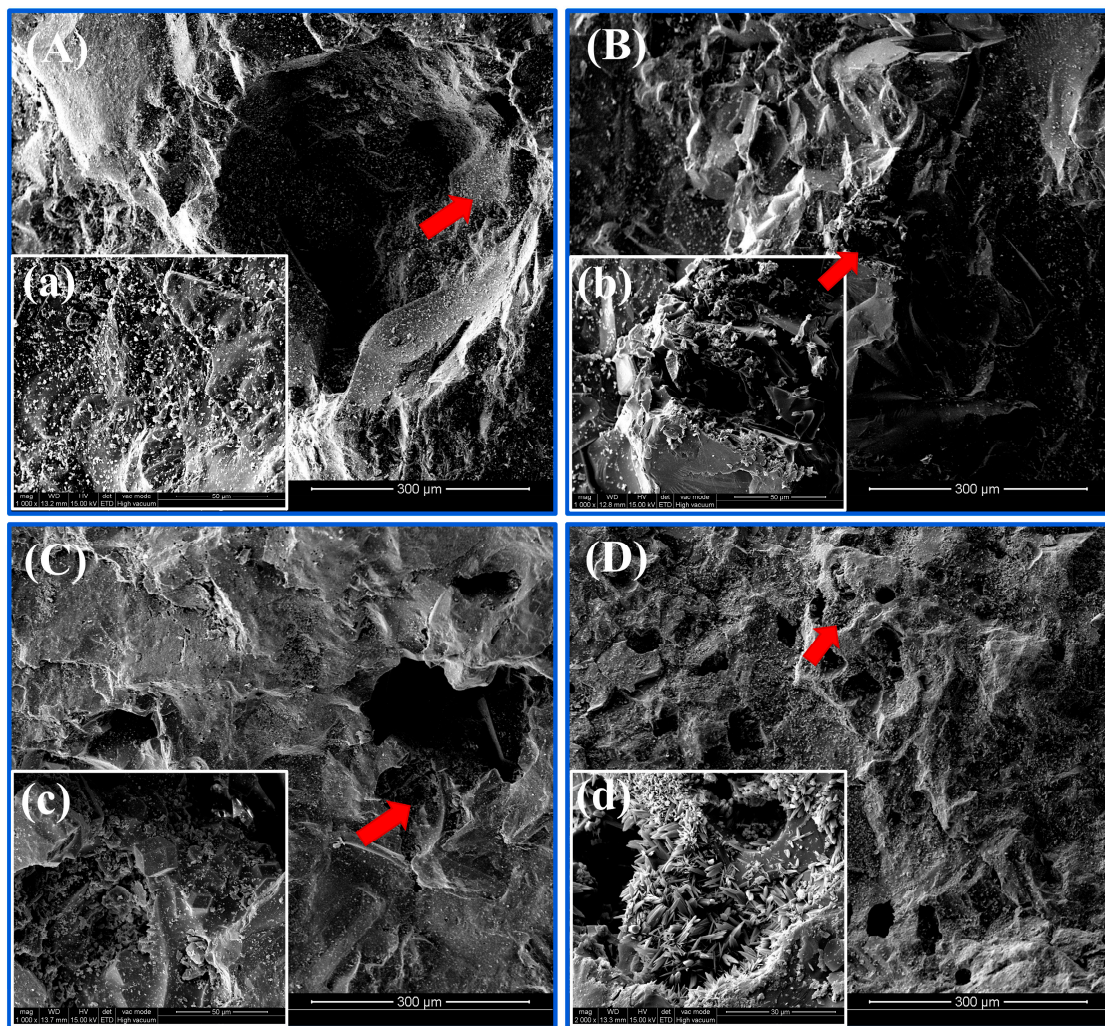


Figure 7. SEM images of the sponge iron samples (A,a) before the reaction and after the reaction at (B,b) pH = 7, (C,c) pH = 3, and (D,d) pH = 10.

The main mechanism of nitrogen and phosphorus co-removal in adsorption experiments was deduced based on experimental results and material characterization, as illustrated in Figure 8. Firstly, protons and NO_3^- were adsorbed on the sponge iron surface when it is introduced to solutions, and sponge iron also released electrons for NO_3^- -N reduction. NO_3^- -N was reduced to NH_4^+ -N and Fe^0 was oxidized to Fe^{3+} and Fe^{2+} . Then, according to the free diffusion theory, phosphate ions in the solution easily diffused to the area with a low concentration. The iron ions constantly dissolving on the sponge iron surface and the phosphate radicals were polar molecules, attracting each other to produce $\text{Fe}_3(\text{PO}_4)_2$ and FePO_4 . The solubility products of $\text{Fe}_3(\text{PO}_4)_2$ and FePO_4 are very small. Therefore, it was easy for them to precipitate and separate from the solution, so as to achieve phosphorus removal. In addition, zeolite removed ammonia nitrogen by cation exchange and physical adsorption.

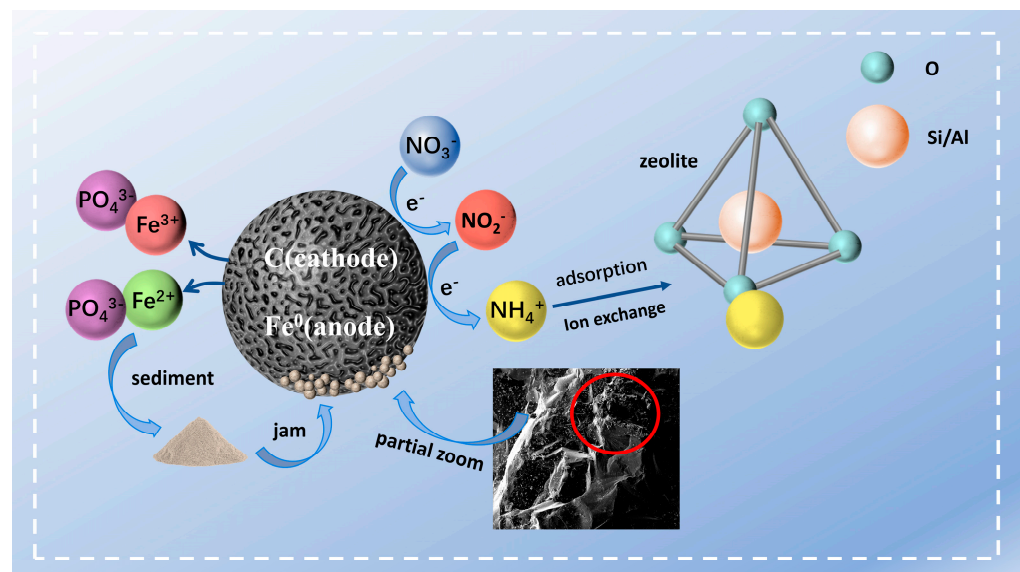


Figure 8. Schematic mechanism of phosphate and nitrogen removal by sponge iron and zeolite.

3.3. Pollutants Removal Performance of CWs

3.3.1. Nitrogen Removal of CWs

The nitrogen removal performance of CW-G and CW-I are shown in Figure 9. During the operational period, the actual influent NH_4^+ -N concentration was about 5.61 ± 0.55 mg/L. Sponge iron was added according to the optimal value obtained in the dosage experiment. The NH_4^+ -N effluent concentration of both CW-G and CW-I consistently remained comparatively low. When the HRT was 24 h, 36 h, and 48 h, the average effluent NH_4^+ -N concentrations of CW-G were 0.07 mg/L, 0.09 mg/L, and 0.19 mg/L, while those of CW-I were 0.07 mg/L, 0.30 mg/L, and 0.88 mg/L. As can be seen from Figure 9b, when HRT was 24 h, the NH_4^+ -N removal efficiencies of CW-G and CW-I were similar and both were higher than 98%. As HRT increased, the NH_4^+ -N effluent concentration of CW-I was significantly higher than that of CW-G. The greater the HRT, the greater the gap between CW-G and CW-I. This phenomenon was attributed to the extended contact time facilitating the complete manifestation of sponge iron's reduction capabilities towards NO_2^- -N and NO_3^- -N.

During the operational period, the actual influent NO_3^- -N concentration was about 10.72 ± 0.66 mg/L. The minimum average effluent NO_3^- -N concentration for both CW-G and CW-I systems occurred at an HRT of 48 h, with values of 5.37 mg/L and 3.53 mg/L (Figure 9c). As HRT increased, the NO_3^- -N removal efficiency of CWs increased significantly, and the NO_3^- -N removal efficiency of CW-I was always higher than that of CW-G. It was evident that an excessively short HRT was not conducive to nitrogen removal in constructed wetlands. This was attributed to the brief residence time of wastewater within the wetland, leading to rapid reoxygenation and inadequate progression of the denitrification reaction. The addition of sponge iron in CW-G facilitates the chemical reduction process, converting NO_3^- -N into NH_4^+ -N effectively. Previous studies have reported that the increase in NO_3^- -N removal efficiency resulting from extending the HRT from 24 h to 48 h was primarily attributed to enhanced chemical effects rather than microbial effects, such as nitrate-dependent ferrous oxidation (NDFO) [25]. The effluent NH_4^+ -N concentration of wetland remained relatively low, with NO_3^- -N constituting the primary component of total nitrogen. Consequently, the effluent TN concentration exhibited a similar trend to that of NO_3^- -N. During the operational period, the actual influent TN concentration was about 15.23 ± 1.05 mg/L. As shown in Figure 9e, the average effluent TN concentrations of both CW-G and CW-I reached the minimum values when HRT was 48 h, which was 5.84 mg/L and 1.01 mg/L, respectively. As HRT increased, the disparity of TN removal efficiency between CW-G and CW-I became larger. Due to the reduction of NO_3^- -N to NH_4^+ -N by sponge iron, the NO_3^- -N effluent concentration was decreased, and the removal efficiency

of NO_3^- -N was raised. Meanwhile, the excellent NH_4^+ -N removal capability of constructed wetlands maintained the effluent NH_4^+ -N concentration at an extremely low level. The TN removal efficiency of CW-I was improved by the combined influence of these factors.

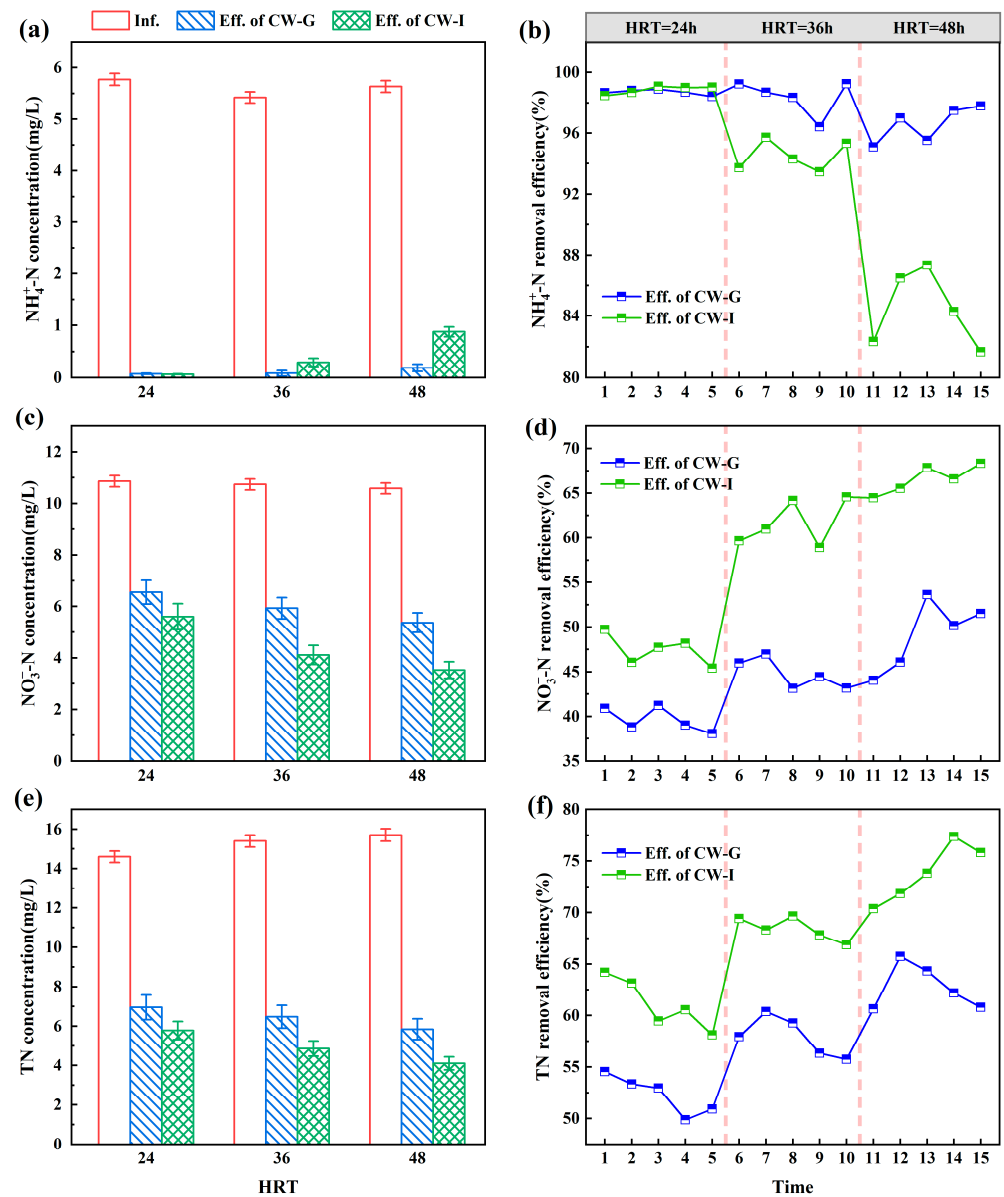


Figure 9. The performances of nitrogen removal in CW-G and CW-I at different HRTs: (a) NH_4^+ -N effluent concentration; (b) NH_4^+ -N removal efficiency; (c) NO_3^- -N effluent concentration; (d) NO_3^- -N removal efficiency; (e) TN effluent concentration; (f) TN removal efficiency.

3.3.2. Phosphorus Removal of CWs

The TP removal performance of CW-G and CW-I are shown in Figure 10. During the operational period, the actual influent TP concentration was about 0.54 ± 0.06 mg/L. When the HRT was 24 h, 36 h, and 48 h, the average effluent TP concentrations of CW-G were 0.50 mg/L, 0.52 mg/L, and 0.49 mg/L, while those of CW-I were 0.46 mg/L, 0.46 mg/L, and 0.42 mg/L, respectively. The minimum average effluent TP concentrations for both CW-G and CW-I were observed at an HRT of 48 h. The variation in TP removal efficiency of CWs was primarily associated with anaerobic phosphorus release by polyphosphate-accumulating organisms and chemical adsorption. From the experimental results, it can be observed that the actual residence time had some impact on TP removal, but the

impact was small. During the whole operation, the TP removal efficiency of CW-I was consistently higher than that of CW-G (Figure 10b), indicating the addition of sponge iron to the system can significantly improve TP removal performance. In the presence of higher dissolved oxygen concentrations, sponge iron can generate more iron hydroxides to bind with phosphate [46]. As the HRT was extended, the improvement in the TP removal efficiency of CW-I was notably greater than that of CW-G. This is attributed to the increased HRT, which also prolongs the reaction time between $\text{PO}_4^{3-}\text{-P}$ and iron. Although CW-I had better TP removal efficiency than CW-G, there was still significant room for improvement. To improve the TP removal efficiency, the dosage of sponge iron can be increased and it can be treated with acid before use.

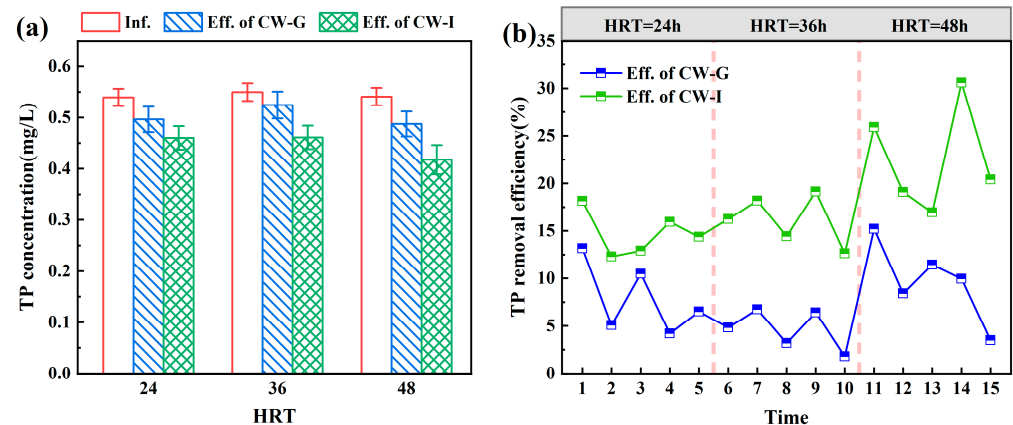


Figure 10. The performances of TP removal in CW-G and CW-I at different HRTs: (a) TP effluent concentration; (b) TP removal efficiency.

4. Conclusions

The impacts of various factors on the synergistic reaction were studied, and it was discovered that removal efficiency improved as solution pH values decreased. The addition of a small quantity of activated carbon to the solution promoted the development of microcells, which produced an iron–carbon micro-electrolysis effect and accelerated the reaction rate. The vertical-flow constructed wetland with sponge iron was established. Under different HRT conditions, the TN removal efficiency of CW-I was 6.08–15.18% higher than that of CW-G, while the TP removal efficiency was 5.00–20.67% higher. The enhancing effect of sponge iron on nitrogen and phosphorus removal was best when the HRT was 48 h. The increase of the HRT not only improved the nitrogen and phosphorus removal effect of constructed wetlands but also enhanced the reduction capacity of iron and the phosphorus removal effect. Chemical reduction is the primary method for removing NO_3^- -N, ion exchange and electrostatic adsorption are the mechanisms for removing NH_4^+ -N, and precipitation formation and partial adsorption are the strategies for removing $\text{PO}_4^{3-}\text{-P}$. This work provides a reference for the simultaneous and deep treatment of phosphate and different forms of nitrogen.

Author Contributions: Y.S.: conceptualization, data curation, formal analysis, writing—original draft; M.H.: validation, investigation, data curation, resources, methodology; Y.X.: methodology, investigation; M.T.: methodology, investigation, writing—review and editing; L.G.: resources; Y.K.: writing—review and editing; S.C.: supervision, resources; Z.J.: conceptualization, project administration, writing—review and editing. All authors have read and agreed to the published version of the manuscript.

Funding: This research received no external funding.

Data Availability Statement: The data presented in this study are available on request from the corresponding author.

Acknowledgments: The authors acknowledge the financial support provided by the Project Funded by the National First-class Disciplines (PNFD); Jiangsu Province Industry-University Research Cooperation Project (BY20230030) and Nanjing Science and Technology Plan for Construction Industry (Ks22420).

Conflicts of Interest: Authors Lin Guan and Yu Kong were employed by the company Nanjing Municipal Design and Research Institute Co., Ltd. The remaining authors declare that the research was conducted in the absence of any commercial or financial relationships that could be construed as a potential conflict of interest.

References

1. Wu, T.; Yang, S.-S.; Zhong, L.; Pang, J.-W.; Zhang, L.; Xia, X.-F.; Yang, F.; Xie, G.-J.; Liu, B.-F.; Ren, N.-Q. Simultaneous nitrification, denitrification and phosphorus removal: What have we done so far and how do we need to do in the future? *Sci. Total Environ.* **2023**, *856*, 158977. [[CrossRef](#)] [[PubMed](#)]
2. Gao, X.; Bi, Y.; Su, L.; Lei, Y.; Gong, L.; Dong, X.; Li, X.; Yan, Z. Unveiling the nitrogen and phosphorus removal potential: Comparative analysis of three coastal wetland plant species in lab-scale constructed wetlands. *J. Environ. Manag.* **2024**, *351*, 119864. [[CrossRef](#)] [[PubMed](#)]
3. Zhao, L.; Fu, D.; Wu, X.; Yuan, X.; Wang, S.; Duan, C. Opposite response of constructed wetland performance in nitrogen and phosphorus removal to short and long terms of operation. *J. Environ. Manag.* **2024**, *351*, 120002. [[CrossRef](#)]
4. Abell, J.M.; Özkundakci, D.; Hamilton, D.P.; Reeves, P. Restoring shallow lakes impaired by eutrophication: Approaches, outcomes, and challenges. *Crit. Rev. Environ. Sci. Technol.* **2020**, *52*, 1199–1246. [[CrossRef](#)]
5. Pandian, A.M.K.; Rajamehala, M.; Singh, M.V.P.; Sarojini, G.; Rajamohan, N. Potential risks and approaches to reduce the toxicity of disinfection by-product—A review. *Sci. Total Environ.* **2022**, *822*, 153323. [[CrossRef](#)]
6. Zhang, H.; Gao, P.; Liu, Y.; Du, Z.; Feng, L.; Zhang, L. Effects of different types of nitrogen sources in water on the formation potentials of nitrogenous disinfection by-products in chloramine disinfection process based on isotope labeling. *Sci. Total Environ.* **2022**, *842*, 156692. [[CrossRef](#)] [[PubMed](#)]
7. Zheng, Z.; Li, W.; Zhang, D.; Qin, W.; Zhao, Y.; Lv, L. Effect of iron and manganese on ammonium removal from micro-polluted source water by immobilized HITLi7(T) at 2 degrees C. *Bioresour. Technol.* **2019**, *285*, 121367. [[CrossRef](#)] [[PubMed](#)]
8. Tabassum, S. A combined treatment method of novel Mass Bio System and ion exchange for the removal of ammonia nitrogen from micro-polluted water bodies. *Chem. Eng. J.* **2019**, *378*, 122217. [[CrossRef](#)]
9. Hord, N.G.; Tang, Y.; Bryan, N.S. Food sources of nitrates and nitrites: The physiologic context for potential health benefits. *Am. J. Clin. Nutr.* **2009**, *90*, 1–10. [[CrossRef](#)]
10. Omar, S.; Webb, A.; Lundberg, J.; Weitzberg, E. Therapeutic effects of inorganic nitrate and nitrite in cardiovascular and metabolic diseases. *J. Intern. Med.* **2016**, *279*, 315–336. [[CrossRef](#)]
11. Liu, S.; Han, X.; Li, S.; Xuan, W.; Wei, A. Stimulating Nitrate Removal with Significant Conversion to Nitrogen Gas Using Biochar-Based Nanoscale Zerovalent Iron Composites. *Water* **2022**, *14*, 2877. [[CrossRef](#)]
12. Zhang, S.; Ali, A.; Su, J.; Huang, T.; Li, M. Performance and enhancement mechanism of redox mediator for nitrate removal in immobilized bioreactor with preponderant microbes. *Water Res.* **2021**, *209*, 117899. [[CrossRef](#)]
13. Florea, A.F.; Lu, C.; Hansen, H.C.B. A zero-valent iron and zeolite filter for nitrate recycling from agricultural drainage water. *Chemosphere* **2022**, *287*, 131993. [[CrossRef](#)] [[PubMed](#)]
14. Wenten, I.G. Reverse osmosis applications: Prospect and challenges. *Desalination* **2016**, *391*, 112–125. [[CrossRef](#)]
15. Winkler, M.K.; Straka, L. New directions in biological nitrogen removal and recovery from wastewater. *Curr. Opin. Biotechnol.* **2019**, *57*, 50–55. [[CrossRef](#)] [[PubMed](#)]
16. Zhang, Z.; Zhang, Y.; Chen, Y. Recent advances in partial denitrification in biological nitrogen removal: From enrichment to application. *Bioresour. Technol.* **2020**, *298*, 122444. [[CrossRef](#)] [[PubMed](#)]
17. Ren, Z.; Jia, B.; Zhang, G.; Fu, X.; Wang, Z.; Wang, P.; Lv, L. Study on adsorption of ammonia nitrogen by iron-loaded activated carbon from low temperature wastewater. *Chemosphere* **2021**, *262*, 127895. [[CrossRef](#)] [[PubMed](#)]
18. Huo, H.; Lin, H.; Dong, Y.; Cheng, H.; Wang, H.; Cao, L. Ammonia-nitrogen and phosphates sorption from simulated reclaimed waters by modified clinoptilolite. *J. Hazard. Mater.* **2012**, *229–230*, 292–297. [[CrossRef](#)] [[PubMed](#)]
19. Zhang, Y.; Douglas, G.B.; Kaksonen, A.H.; Cui, L.; Ye, Z. Microbial reduction of nitrate in the presence of zero-valent iron. *Sci. Total Environ.* **2019**, *646*, 1195–1203. [[CrossRef](#)]
20. Wang, J.; Li, Z.; Wang, Q.; Lei, Z.; Yuan, T.; Shimizu, K.; Zhang, Z.; Adachi, Y.; Lee, D.J.; Chen, R. Achieving stably enhanced biological phosphorus removal from aerobic granular sludge system via phosphorus rich liquid extraction during anaerobic period. *Bioresour. Technol.* **2022**, *346*, 126439. [[CrossRef](#)]
21. Chen, L.; Chen, H.; Hu, Z.; Tian, Y.; Wang, C.; Xie, P.; Deng, X.; Zhang, Y.; Tang, X.; Lin, X.; et al. Carbon uptake bioenergetics of PAOs and GAOs in full-scale enhanced biological phosphorus removal systems. *Water Res.* **2022**, *216*, 118258. [[CrossRef](#)] [[PubMed](#)]
22. Wu, H.; Wang, R.; Yan, P.; Wu, S.; Chen, Z.; Zhao, Y.; Cheng, C.; Hu, Z.; Zhuang, L.; Guo, Z. Constructed wetlands for pollution control. *Nat. Rev. Earth Environ.* **2023**, *4*, 218–234. [[CrossRef](#)]

23. Xue, R.; Xu, J.; Gu, L.; Pan, L.; He, Q. Study of Phosphorus Removal by Using Sponge Iron Adsorption. *Water Air Soil. Pollut.* **2018**, *229*, 161. [[CrossRef](#)]
24. Mejia, J.; Roden, E.E.; Ginder-Vogel, M. Influence of Oxygen and Nitrate on Fe (Hydr)oxide Mineral Transformation and Soil Microbial Communities during Redox Cycling. *Environ. Sci. Technol.* **2016**, *50*, 3580–3588. [[CrossRef](#)] [[PubMed](#)]
25. Li, J.; Zeng, W.; Liu, H.; Wu, Y.; Miao, H. Performances and mechanisms of simultaneous nitrate and phosphate removal in sponge iron biofilter. *Bioresour. Technol.* **2021**, *337*, 125390. [[CrossRef](#)] [[PubMed](#)]
26. Zeng, Y.; Walker, H.; Zhu, Q. Reduction of nitrate by NaY zeolite supported Fe, Cu/Fe and Mn/Fe nanoparticles. *J. Hazard. Mater.* **2017**, *324*, 605–616. [[CrossRef](#)]
27. Diao, Z.H.; Qian, W.; Lei, Z.X.; Kong, L.J.; Du, J.J.; Liu, H.; Yang, J.W.; Pu, S.Y. Insights on the nitrate reduction and norfloxacin oxidation over a novel nanoscale zero valent iron particle: Reactivity, products, and mechanism. *Sci. Total Environ.* **2019**, *660*, 541–549. [[CrossRef](#)]
28. Tian, H.; Huang, C.; Wang, P.; Wei, J.; Li, X.; Zhang, R.; Ling, D.; Feng, C.; Liu, H.; Wang, M. Enhanced elimination of Cr (VI) from aqueous media by polyethyleneimine modified corn straw biochar supported sulfide nanoscale zero valent iron: Performance and mechanism. *Bioresour. Technol.* **2023**, *369*, 128452. [[CrossRef](#)] [[PubMed](#)]
29. Sun, Z.; Xu, Z.; Zhou, Y.; Zhang, D.; Chen, W. Effects of different scrap iron as anode in Fe-C micro-electrolysis system for textile wastewater degradation. *Environ. Sci. Pollut. Res. Int.* **2019**, *26*, 26869–26882. [[CrossRef](#)]
30. Stroka, J.R.; Kandemir, B.; Matson, E.M.; Bren, K.L. Electrocatalytic Multielectron Nitrite Reduction in Water by an Iron Complex. *ACS Catal.* **2020**, *10*, 13968–13972. [[CrossRef](#)]
31. Huang, Y.H.; Zhang, T.C. Effects of low pH on nitrate reduction by iron powder. *Water Res.* **2004**, *38*, 2631–2642. [[CrossRef](#)] [[PubMed](#)]
32. Guo, X.; Yang, Z.; Liu, H.; Lv, X.; Tu, Q.; Ren, Q.; Xia, X.; Jing, C. Common oxidants activate the reactivity of zero-valent iron (ZVI) and hence remarkably enhance nitrate reduction from water. *Sep. Purif. Technol.* **2015**, *146*, 227–234. [[CrossRef](#)]
33. Xu, J.; Hao, Z.; Xie, C.; Lv, X.; Yang, Y.; Xu, X. Promotion effect of Fe²⁺ and Fe₃O₄ on nitrate reduction using zero-valent iron. *Desalination* **2012**, *284*, 9–13. [[CrossRef](#)]
34. Ju, Y.; Liu, X.; Liu, R.; Li, G.; Wang, X.; Yang, Y.; Wei, D.; Fang, J.; Dionysiou, D.D. Environmental application of millimeter-scale sponge iron (s-Fe(0)) particles (II): The effect of surface copper. *J. Hazard. Mater.* **2015**, *287*, 325–334. [[CrossRef](#)]
35. Hou, L.; Liang, Q.; Wang, F. Mechanisms that control the adsorption–desorption behavior of phosphate on magnetite nanoparticles: The role of particle size and surface chemistry characteristics. *RSC Adv.* **2020**, *10*, 2378–2388. [[CrossRef](#)] [[PubMed](#)]
36. Yin, Q.; Wang, R.; Zhao, Z. Application of Mg–Al-modified biochar for simultaneous removal of ammonium, nitrate, and phosphate from eutrophic water. *J. Clean. Prod.* **2018**, *176*, 230–240. [[CrossRef](#)]
37. Zhang, X.; Song, Z.; Dou, Y.; Xue, Y.; Ji, Y.; Tang, Y.; Hu, M. Removal difference of Cr(VI) by modified zeolites coated with MgAl and ZnAl-layered double hydroxides: Efficiency, factors and mechanism. *Colloids Surf. A Physicochem. Eng. Asp.* **2021**, *621*, 126583. [[CrossRef](#)]
38. Seftel, E.M.; Ciocarlan, R.G.; Michielsen, B.; Meynen, V.; Mullens, S.; Cool, P. Insights into phosphate adsorption behavior on structurally modified ZnAl layered double hydroxides. *Appl. Clay Sci.* **2018**, *165*, 234–246. [[CrossRef](#)]
39. Tseng, R.L.; Wu, F.C. Inferring the favorable adsorption level and the concurrent multi-stage process with the Freundlich constant. *J. Hazard. Mater.* **2008**, *155*, 277–287. [[CrossRef](#)]
40. Wang, Y.; Song, X.; Xu, Z.; Cao, X.; Song, J.; Huang, W.; Ge, X.; Wang, H. Adsorption of Nitrate and Ammonium from Water Simultaneously Using Composite Adsorbents Constructed with Functionalized Biochar and Modified Zeolite. *Water Air Soil. Pollut.* **2021**, *232*, 198. [[CrossRef](#)]
41. Jellali, S.; Wahab, M.A.; Hassine, R.B.; Hamzaoui, A.H.; Bousselmi, L. Adsorption characteristics of phosphorus from aqueous solutions onto phosphate mine wastes. *Chem. Eng. J.* **2011**, *169*, 157–165. [[CrossRef](#)]
42. Si, Z.; Song, X.; Wang, Y.; Cao, X.; Wang, Y.; Zhao, Y.; Ge, X.; Sand, W. Untangling the nitrate removal pathways for a constructed wetland- sponge iron coupled system and the impacts of sponge iron on a wetland ecosystem. *J. Hazard. Mater.* **2020**, *393*, 122407. [[CrossRef](#)] [[PubMed](#)]
43. Wahab, M.A.; Boubakri, H.; Jellali, S.; Jedidi, N. Characterization of ammonium retention processes onto cactus leaves fibers using FTIR, EDX and SEM analysis. *J. Hazard. Mater.* **2012**, *241–242*, 101–109. [[CrossRef](#)] [[PubMed](#)]
44. He, Y.; Lin, H.; Dong, Y.; Liu, Q.; Wang, L. Simultaneous removal of ammonium and phosphate by alkaline-activated and lanthanum-impregnated zeolite. *Chemosphere* **2016**, *164*, 387–395. [[CrossRef](#)] [[PubMed](#)]
45. Boeykens, S.P.; Piol, M.N.; Samudio Legal, L.; Saralegui, A.B.; Vazquez, C. Eutrophication decrease: Phosphate adsorption processes in presence of nitrates. *J. Environ. Manag.* **2017**, *203*, 888–895. [[CrossRef](#)]
46. Narayanasamydamodaran, S.; Zuo, J.E.; Ren, H.; Kumar, N. Scrap Iron Filings assisted nitrate and phosphate removal in low C/N waters using mixed microbial culture. *Front. Environ. Sci. Eng.* **2021**, *15*, 66. [[CrossRef](#)]

Disclaimer/Publisher’s Note: The statements, opinions and data contained in all publications are solely those of the individual author(s) and contributor(s) and not of MDPI and/or the editor(s). MDPI and/or the editor(s) disclaim responsibility for any injury to people or property resulting from any ideas, methods, instructions or products referred to in the content.